ACS OMEGA

http://pubs.acs.org/journal/acsodf

Article

Phosphorous-Doped Graphitic Material as a Solid Acid Catalyst for Microwave-Assisted Synthesis of β-Ketoenamines and Baeyer–Villiger Oxidation

Sayantan Maity, Farsa Ram, and Basab Bijayi Dhar*

Cite This: *ACS Omega* 2020, 5, 15962−15972

Read Online

ACCESS | Metrics & More | Article Recommendations | Supporting Information

ABSTRACT: Synthesis of phosphorous-doped graphitic materials (P-Gc) using phytic acid as a precursor was done in a microwave oven in a cost- and time-effective green way. The material was used as a solid acid catalyst for microwave (MW)-assisted synthesis of β-ketoenamines and Baeyer−Villiger (BV) oxidation. In the case of BV oxidation, hydrogen peroxide (H_2O_2) was used as a green oxidant. For β-ketoenamines, in most cases, 100% conversion with an ∼95% yield was achieved in ethyl acetate medium. In solvent-free conditions, the yield of β-ketoenamines was ∼75%. A kinetic study suggested that the resonance stabilization of the positive reaction center happens in the transition state for β-ketoenamine synthesis. In BV oxidation, cyclic ketones were converted to their corresponding cyclic esters in good to high yields (∼80% yield) in a shorter reaction time (6−20 min). As per our knowledge, this is the first report of BV oxidation catalyzed by a heteroatom-doped graphitic material. For BV oxidation, the phosphoric acid functional groups present in P-Gc might increase the electrophilicity of the carbonyl group of the ketones to compensate for the weakness of H_2O_2 as a nucleophile and a spiro-bisperoxide intermediate has been identified in high-resolution mass spectrometry.

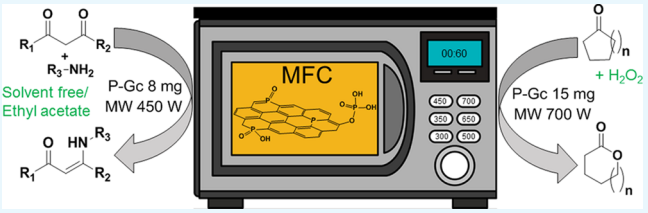

INTRODUCTION

Developing inexpensive non-polluting catalysts to produce high value-added chemicals is a significant task in many important industrial and fine chemical processes. Widely used metal-catalysts are expensive and treacherous, having time-consuming synthetic methods, and the recovery process is complicated. Therefore, the application and design of metal-free catalysts (MFCs) for chemical transformation is demanding from the view of basic and applied research.[1,2] In addition to this, nonconventional energy sources such as microwave (MW), ultrasonic irradiation, and mechanochemical mixing have been popularized to overcome problems associated with excessive and wasteful heating in conventional refluxing methods.[3] Solvent-free strategies are also gaining attraction to develop a cleaner process.[4]

Graphitic or graphene-based materials are newly emerging green MFCs. These are used in various chemical transformations because of their large surface area, easy surface functionalization, tunable surface wettability, long-lasting stability, conductivity, and reusability.[2,5] The giant π structures of graphene promote a strong interaction with the π-framework of reactants and accelerate the reaction rate.[6] The physiochemical, redox, and electronic properties of graphene can be drastically altered by doping various heteroatoms like boron, nitrogen, oxygen, phosphorous, sulfur, etc. Graphene oxide (GO) and carbon materials doped with nitrogen (N) and boron (B) have been explored for various applications[7,8] compared to heavier atoms as dopant. P doping in graphene creates more structural distortions of the hexagonal carbon framework,[9] and it has been reported that P-doped bilayer graphene exhibits five times more electron mobility compared to pristine bi-layer graphene.[9d] Recently, Patel et al. reported benzyl alcohol oxidation using P-doped carbonaceous materials.[10]

Here, we are reporting the microwave-assisted (MW-assisted) synthesis of a P-doped graphitic material (P-Gc) using phytic acid as a precursor by a reported method with some modifications.[10] The P content in our synthesized material is 3.93 wt %, and the specific surface area is 1635 m^2/g. The well-characterized P-Gc was used as a solid catalyst in MW-assisted synthesis of β-ketoenamines in ethyl acetate medium. β-Ketoenamine is a highly efficient antitumor,[11] antibacterial,[12] and anti-inflammatory[13] agent. In most cases, we achieved more than 95% yields and the average reaction time was 3−5 min only. In traditional oil bath (OB) heating, we achieved an ∼88% yield of β-ketoenamines within 1 h. However, in a solvent-free condition, the MW-assisted conversion was ∼75% in most cases. To the best of our knowledge, this is the fastest approach to date for β-

Received: March 19, 2020
Accepted: June 8, 2020
Published: June 24, 2020

ketoenamine synthesis using a heteroatom-doped carbocatalyst with a maximum yield. Very recently, industrial-quality GO as a catalyst in an oil bath (reaction time ≥ 3 h) has been reported.[14] A GO−SnO_2 nanocomposite has also been used for the same reaction with and without a solvent.[15] However, the second one is not completely metal-free.

Using the same carbocatalyst, MW-assisted Baeyer−Villiger (BV) oxidations were also efficiently performed for a wide range of ketones using hydrogen peroxide (H_2O_2) as a green oxidant. The direct use of H_2O_2 simplifies the operational condition and minimizes the production of waste. Commonly, expensive organic peracids are used in BV reactions because H_2O_2 is a weak nucleophile, hence kinetically very inert compare to peracids.[16] In our case, acid groups present in the P-Gc improve the electrophilicity of the carbonyl group of the ketones to compensate for the weakness. In contrast to peracids, H_2O_2 is safe, inexpensive, and contains more active oxygen atoms. In recent years, some successful attempts have been made using various homogeneous transition-metal and main group-metal catalysts, organocatalysts, and heterogeneous catalysts to activate H_2O_2 in BV oxidation.[17] Using our methodology, in contrast to aromatic ketones, cyclic ketones were converted to their corresponding cyclic esters in good to high yields (∼80%). As per our knowledge, this is the first report of BV oxidation catalyzed by a heteroatom-doped graphitic material using H_2O_2 as an oxidant.

EXPERIMENT

Materials and Characterization. All chemicals were purchased from Sigma-Aldrich or Alfa and used without further purification.

P-Gc was characterized by powder X-ray diffraction (PXRD), Fourier transform infrared (FTIR), Raman spectrometry, scanning electron microscopy (SEM), transmission electron microscopy (TEM), atomic force microscopy (AFM), Brunauer−Emmett−Teller (BET) analysis, and X-ray photoelectron spectroscopy (XPS). PXRD was obtained using a Rigaku PXRD instrument. FTIR data were recorded using a Nicolte iS5 FTIR spectrometer (Thermo Fisher Scientific), and the Raman spectrum was recorded using a Horiba Raman spectrophotometer. TEM imaging was performed on a Cu grid at an accelerating voltage of 200 kV using TALOS S-FEG TEM. The elemental microanalysis of P-Gc was done using a Nova Nano SEM 450 (FEI) scanning electron microscope, coupled with energy-dispersive analytical X-ray spectroscopy (EDS). Surface topography images of P-Gc were obtained from AFM XE7, Park System. XPS was measured in ESCA, Omicron Nanotechnology, Oxford Instruments, and the binding energies were calculated using the maximum intensity of the C 1s signal at 284.8 eV as the reference. BET analysis was conducted in a Quantachrome autosorb automated gas sorption system using a nitrogen gas at 77 K to calculate the specific surface area. ^{13}C NMR and ^{1}H NMR spectra were recorded on Bruker spectrometer operating at 400 MHz. Chloroform-d ($CDCl_3$) was used as a solvent, and tetramethylsilane (TMS) was employed as an internal reference.

Synthesis of the Catalyst. In a 20 mL quartz crucible, 500 μL of 50% aqueous solution of phytic acid was taken and irradiated in a multimodal scientific microwave oven with a stirring facility (model: RG 31L from Raga Tech, India; input voltage: 220 to 240 V; input frequency: 50 Hz; output frequency: 2450 MHz) for 40 s in 450 W power. The resultant black solution was cooled, washed with water, and dried in an oven. The material was mostly of a flake type. The material was grinded (made into small pieces) using a mortar and pestle and then ultrasonicated in water for 15 min. The residue was collected by vacuum filtration using a G3 sintered glass crucible. Then, the crucible was placed in the oven at 70 °C for drying (Scheme S1). In our modified method, we have enhanced the ultrasonication time (three times) from the previous report.[10]

Synthesis of β-Ketoenamines. In a 20 mL quartz crucible P-Gc (8 mg), a β-diketo compound (1 mmol) and amines (1 mmol) were mixed and kept in a multimodal microwave oven (RG 31L) at 450 W at 60 °C for 2−4 min with continuous stirring with a magnetic bead using ethyl acetate as solvent to get β-ketoenamine. Using the same solvent, reactions were also done in conventional OB heating at 60 °C for 40−90 min with 10 mg of P-Gc. The reaction was monitored by thin-layer chromatography. The products were purified using a silica column. The mixture of ethyl acetate and hexane was used to run the column. ^{1}H and ^{13}C NMR spectra and a mass spectrum (HR-MS) m/z were taken for the products. The reactions were performed in solvent-free conditions in both the MW and traditional OB. Products are purified on a silica gel column (100−120 mesh size), and then the isolated yield was calculated. Conversion and percent yields were also measured using high-performance liquid chromatography (HPLC, Figure S16).

Baeyer−Villiger Oxidation. In a 20 mL quartz crucible, P-Gc (15 mg), ketone (1 mmol), and H_2O_2 (50% aqueous; 1.3 mmol) were mixed and kept in a multimodal scientific microwave oven (RG 31L) at 700 W at 80 °C using acetonitrile, ethanol, and 1,2-dichloroethane (2 mL) as solvent to get lactones or esters. Depending on the substrate, reactions went on for 6−50 min. In the OB, it took 2−12 h keeping the other parameters unchanged. In the case of aromatic ketones, conversion and yields were measured using HPLC. For non-aromatic ketones, the product was separated using column chromatography and then the isolated yield was calculated.

Catalyst Recyclability. The catalyst was recovered easily through centrifugation. The recovered catalyst was washed with solvent and dried at 60 °C. Recyclability of the catalyst was carried for synthesis of β-ketoenamines (e.g., the product from 1,1,1-trifluoro-2,4-pentanedione and para-anisidine) and BV oxidation (e.g., the product from 4-*tert*-butylcyclohexanone and 50% H_2O_2) in both the MW and OB for up to five cycles.

Kinetic Studies. A kinetic study of microwave-assisted synthesis of β-ketoenamine was done in a Cary 8454 UV−vis spectrophotometer in a 1 cm quartz cell at room temperature to gain further insight into the reaction mechanism. The rates of product formation of 1,1,1-trifluoro-2,4-pentanedione and various *para* and *meta*-substituted anilines in ethyl acetate were monitored as a function of time. Six reactions in each case were irradiated for six different periods at 10, 20, 30, 40, 50, and 60 s. Then, catalyst separation was done by syringe filtration and proper dilution was made using ethylacetate. All the reactions were repeated three times. The product peaks did not overlap with those of the reactants. Kinetic experiments were also performed by varying the β-diketo compounds with aniline. The effect of solvents on the rate was also checked.

In the case of microwave-assisted BV oxidation of cyclic ketones, as the reagents and products are UV inactive, the reaction kinetics was monitored through ^{1}H NMR spectroscopy following the appearance of a triplet peak between δ =

https://dx.doi.org/10.1021/acsomega.0c01231
ACS Omega 2020, 5, 15962−15972

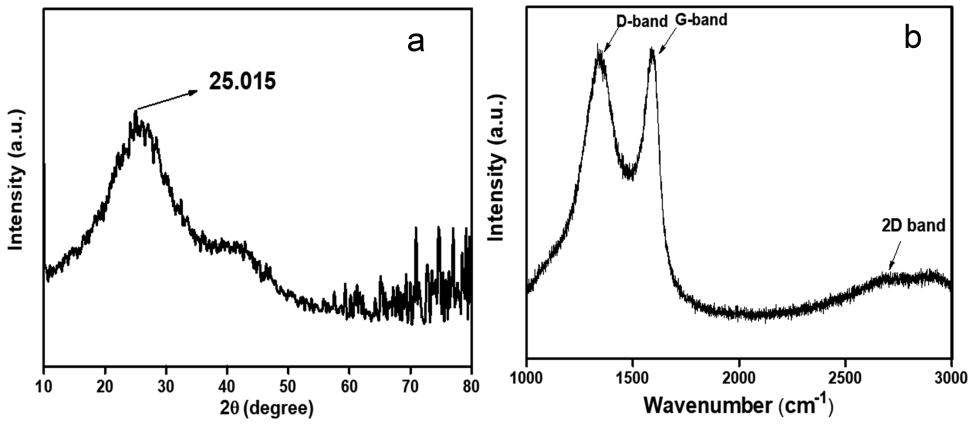

Figure 1. Characterizations of P-Gc: (a) P-XRD pattern and (b) Raman scattering.

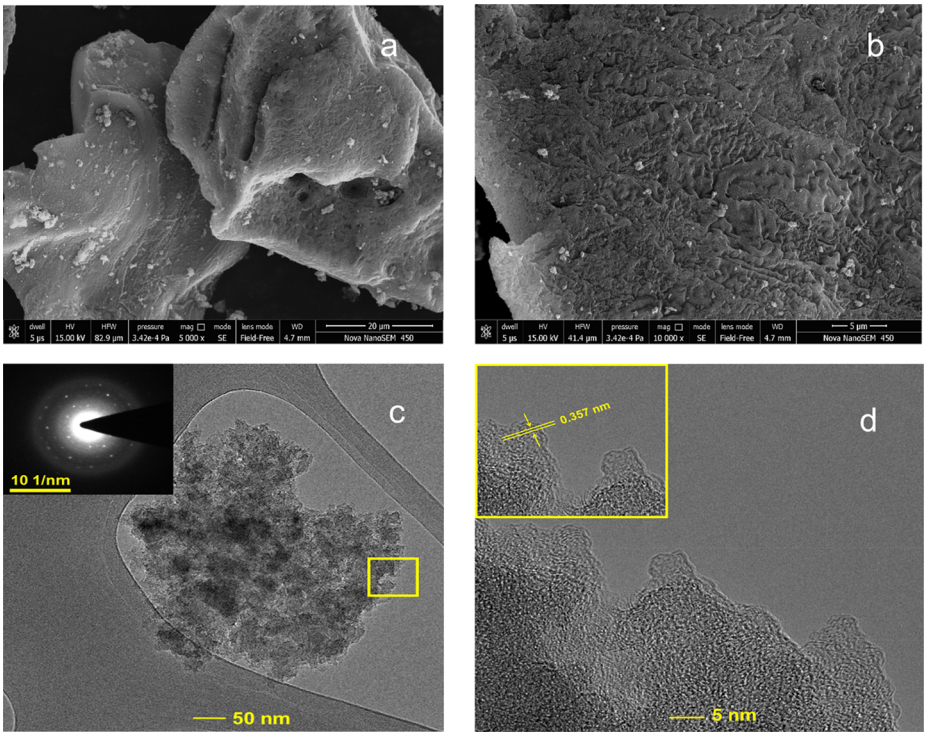

Figure 2. (a) SEM Image (20 μm scale bar), (b) SEM image (5 μm scale bar), (c) TEM image (50 nm resolution), inset: SAED pattern, (d) TEM image (5 nm scale bar), inset: interlayer distance.

4.25 and 4.40 in δ-valerolactone (product from cyclopentanone) and δ = 4.18 and 4.30 in ε-caprolactone (product from cyclohexanone). In the case of (1*R*,3*R*,8*S*)-4-oxatricyclo-[4.3.1.1]undecan-5-one (product from 2-adamantanone), it is a multiplet between δ = 4.45 and 4.55. At first, a series of solutions containing different known concentrations of the products were run using $CDCl_3$ as solvent and equal volumes of mesitylene as internal reference. The number of protons from the singlet aromatic peak in mesitylene between δ = 6.73 and 6.86 was set as "1" for all the solutions. With reference to this, the triplet peak was integrated and plotted against corresponding concentrations of the product. Using the slope of this calibration curve, the concentration of the reaction mixture in different time intervals (1, 2, 3, 4, and 5 min) was calculated from the same triplet/multiplet peak in the ^{1}H NMR spectrum. Each of the aliquots was taken and diluted equally. The volume of mesitylene and total volume of the solution (20 and 500 μL, respectively) were maintained throughout the study. Catalyst separation was done using by syringe filtration, and acetonitrile was separated through vaporization under reduced pressure before NMR sample preparation.

RESULTS AND DISCUSSION

PXRD. The graphitic nature of the material is confirmed by PXRD analysis using Cu Kα as the energy source (λ = 1.542 Å). It shows a sharp peak at 2θ = 25.015 (Figure 1a), which corresponds to the (002) plane, indicating 3.56 Å of the interlayer distance, a slightly increased interlayer spacing compared to graphite (3.36 Å).[9a,18] A very weak peak is observed at 2θ = 42.83 from the (010) plane.[9a]

FTIR and Raman. FTIR analysis of both flakes and sonicated P-Gc shows the presence of C═C, P═O, P−O, C−O, P−OH, and P−C bonds[19] (Figure S1). Raman scattering

https://dx.doi.org/10.1021/acsomega.0c01231
ACS Omega 2020, 5, 15962−15972

(Figure 1b) shows two separate peaks at 1346 and 1586 cm^{-1}, referring to two characteristic bands D and G, which signify the out-of-plane vibration attributed to the presence of structural defects and in-plane vibration of sp^2-bonded carbon atoms, respectively.[19b,20] The ratio of the intensities of these two, I_D/I_G, is found to be 1.025 indicating a high level of disorder in the material.[9a,21] There is also a broad and shorter 2D band near 2689 cm^{-1}.[21] The lower intensity of this band supports the presence of disorder in the graphite layer, which minimizes the chance of a second-order overtone.

SEM, TEM, and AFM. The SEM image (Figure 2a,b and Figure S2) shows that P-Gc consists of pores with wrinkled graphene-like sheets. The wrinkled structure suggests local geometrical distortions and it is possibly due to incorporation of larger P atoms compared to C atoms. EDS analysis shows that the P loading is 3.93 wt % (Table S1 and Figure S3). The TEM image (Figure 2c) shows that the material is amorphous and layers agglomerated heterogeneously. However, the discrete diffraction spots of few layers in the SAED pattern (Figure 2c, inset) confirms the presence of hexagonality, which is attributed to the material's graphitic nature.[18c,21] Graphitic layers were visible only in 5 nm resolution. Then, using Image J software, we measured the interlayer distance (Figure 2d). It was found to be 3.57 Å,[9d,18a,21] which matches the magnitude found in P-XRD (3.56 Å). Similarly, from another selected area, the interlayer distance is obtained as 3.52 Å (Figure S4). The surface roughness of P-Gc is quantified through AFM in the non-contact mode using XEI software. The topography images are shown in Figure S5, and roughness values of the marked areas are presented in Table S2.

BET Analysis. The BET analysis was done using liquid N_2 (cross-sectional area = 16.2 $Å^2$/molecule) as an adsorbate at 77.35 K within the relative pressure range of 0.05 to 1.0. The specific surface area was measured to be 1635 m^2/g (Figure S7a and Table S3). To the best of our knowledge, this is the highest value among multilayered bulk graphite materials reported so far (Table S4).[10,22] According to de Boer's thickness method, the micro-pore area of the P-doped material was 1150 m^2/g and its volume was 0.5988 cc/g. The average pore diameter was 3.263 nm (Figure S7b).

XPS Analysis. The XPS spectra showed that the P-Gc material contains three elements, C, O, and P. The curve fitting was done through XPS peak software using a Gaussian peak shape. The presence of different functional groups of C, O, and P was ascertained from deconvolution of their spectra (Table 1 and Figure 3).[10,23] Atomic percentages of C, O, and P are presented in Table S5.

β-Ketoenamine Synthesis. The optimization of the reaction conditions (Table 2) in MW and OB was done using acetylacetone (1 mmol) and para-anisidine (1 mmol) as reactants in various solvents. In the case of MW heating, an ∼95% yield was observed at 450 W within 3 min in ethyl acetate (entry 4, Table 2, 8 mg of catalyst loading), which is a green solvent according to the environmental and health risk (EHS) assessment[24] of organic solvents. In the solvent-free condition, the catalyst loading was 6 mg and a 78% yield was observed (entry 6, Table 2). In the solvent-free condition in MW, if the catalyst loading was more than 6 mg, we observed that the released heat causes the P-Gc to ignite after a few seconds of the reaction, and as the prime microwave absorber solvent was absent, the entire irradiation was soaked by P-Gc. A lower yield was found in solvent-free conditions, possibly because the catalyst loading was less. At 60 °C in the OB, after 1 h of heating, an 88% yield was noticed in ethyl acetate (100% selectivity, entry 9, Table 2), while a 70% yield was observed in solvent-free conditions (entry 11, Table 2). In MW heating, a lesser yield was noticed in hexane because hexane is transparent to MW (entries 3 and 5, Table 2) and dispersion of P-Gc was less in hexane compared to a polar solvent like ethyl acetate. In the absence of P-Gc, no product was observed in both MW and the OB (entries 7 and 12, Table 2). Reactions using 1 mM phosphoric acid (H_3PO_4) instead of P-Gc in the same conditions give less than 10% isolated yields, indicating the effectiveness of P-Gc as a catalyst over H_3PO_4.

Table 1. Relative Percentages of Functional Groups of C, O, and P Obtained from XPS of P-Gc

O-functional groups	area	contribution
quinone	610	11.31%
C═O, P═O	1419	26.31%
C−O, P−O−C	2217	41.08%
C−OH, P−OH	987	18.30%
COOH	162	3.00%
P-functional groups	**area**	**contribution**
$(Ar)_3P(=O)$	197	26%
$(Ar)_2P(O)(OH)$	400	53%
$-COP(O)(OH)_2$	163	21%
C-functional groups	**area**	**contribution**
C═C	18,339	46.32%
C−P, C−C	4393	11.1%
C−OH	6559	16.5%
C═O	5431	13.71%
COOH	4872	12.31%

The results (Table 3) confirmed that a wide range of aromatic, aliphatic, and cyclic amines could be effectively condensed with various symmetric and asymmetric β-diketones or β-ketoesters. The maximum yield for β-ketoenamines was found for para-substituted anilines with electron-donating groups like $-CH_3$ and $-OCH_3$. Also, for the same aniline, we got the maximum yield in the case of 1,1,1-trifluoro-2,4-pentanedione compared to the other two β-diketo substrates. The yield of β-ketoenamines with *meta*-substituted anilines was found to be less than that of *para*-substituted aniline. A 45% yield of β-ketoenamine was observed for sterically hindered 2-chloroaniline with 1,1,1-trifluoro 2,4 pentanedione in MW conditions (42% yield in the OB). In the case of aliphatic amines like *n*-butylamine and cyclohexylamine, an ∼95% yield was observed.

P-Gc before sonication was also applied to three different reactions (R_1 = $-CH_3$, $-CF_3$, and $-OCH_3$, while R_3 = Ph), giving a lesser yield compared to P-Gc after sonication (Table S6). It suggested that a larger surface area (1635 m^2/g for sonicated and 1077 m^2/g for flakes) is important for catalysis as it provides better exposure of the catalytic site to the substrates.

Mechanistic Understanding of β-Ketoenamine Synthesis Using P-Gc. The log k_{rel} ($k_{rel} = R_X/R_H$, R stands for the rate (Figure S9f) in MW conditions in ethyl acetate) value for aniline and its *para*-substituted analogue was plotted against Hammett parameters, and the ρ value −0.86254 was obtained from the slope (Figure 4). It suggested that electron-donating groups in *para*-substituted anilines accelerate the rate of the reaction by resonance stabilization of the positive reaction

https://dx.doi.org/10.1021/acsomega.0c01231
ACS Omega 2020, 5, 15962−15972

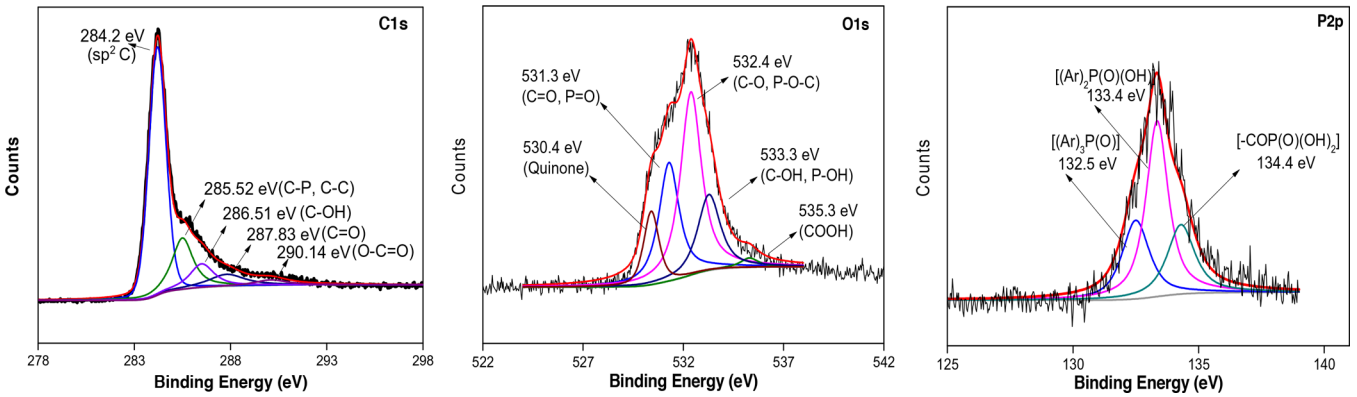

Figure 3. Deconvoluted XPS peaks for C 1s, O 1s, and P 2p in P-Gc.

Table 2. Optimization of Reaction Conditions for β-Ketoenamine Synthesis[a,b]

entry	P-Gc (mg)	temp (°C)	solvent	heating technique	yield (%)
1	4	50	ethyl acetate	MW, 250 W, 3 min	30
2	4	60	ethyl acetate	MW, 450 W, 3 min	63
3	4	60	hexane	MW, 450 W, 3 min	55
4	8	60	ethyl acetate	MW, 450 W, 3 min	95
5	8	60	hexane	MW, 450 W, 3 min	85
6[c]	8	60		MW, 450 W, 3 min	78
7		60	ethyl acetate	MW, 450 W, 3 min	00
8	10	45	ethyl acetate	OB, 45 min	73
9	10	60	ethyl acetate	OB, 60 min	88
10[d]	60	60	ethyl acetate	OB, 60 min	82
11[c]	10	60		OB, 60 min	70
12		60	ethyl acetate	OB, 60 min	00

[a]Selectivity of 100%. [b]MW-assisted reactions; β-diketones or β-ketoesters were taken with a little excess as they readily reach boiling temperatures after absorbing microwave. [c]Solvent-free conditions. [d]Reactants are taken in 10 mmol.

center in transition state 1 (TS1, Figure 5) and the reaction is definitely acid-catalyzed. The conjugate acid of the carbonyl compound has a carbocation character, and the strong C═O bond breaking is the key step. In the case of *meta*-substituted anilines, the linear-free energy relation was not sensitive (Figure S9g).

Based on related mechanisms reported in the literature[14,25] and our observations, we are proposing that β-ketoenamine synthesis goes through the enol form of the β-diketo compounds (Figure 5). Babu et al. mentioned that, even in the absence of any catalyst, the enol form of acetylacetone reacts with aniline.[25a] In general, acid makes the carbonyl carbon more electrophilic and increases the acidity of α-protons, which facilitates enolization.[26a,b] Here, our assumption is that acidic functional groups on P-Gc could favor the enol formation step. These enol forms have quasi-aromatic structures,[26c,d] and the stability follows the trend of $R_1 = CF_3 > CH_3 > OCH_3$.[26c] The rates of MW-assisted reactions of these three β-diketo compounds with aniline were measured to be consistent with this trend, 27.72, 23.74, and 22.21 mol/L/s (Figure S9c−e). It is also suggested in the present case that the reactive form of the β-diketo compound is the enol form.[14,25] The quasi-aromatic structure of the enol form may have π−π interactions with the P-Gc surface (~46% sp^2 C═C and ~11% sp^3 C−C or C−P according to XPS) as aromatic molecules are reported to interact better on graphene surfaces than aliphatic ones.[27]

In order to further test, we performed a reaction in OB conditions taking one equivalent each of acetylacetone, aniline, and cyclohexylamine and studied the reaction using HPLC (Figure S17a). Cyclohexylamine is a stronger nucleophile than aniline. The yield of β-ketoenamine would be expected to be higher from the cyclohexylamine if nucleophilicity is the only governing factor, but the β-ketoenamine yield from aniline was more than 74%. The same experiment was done with *n*-butylamine instead of cyclohexylamine, which is an even stronger nucleophile than cyclohexylamine and has a more flexible structure. However, in this case, generated β-ketoenamine from aniline was more (~55%) compared to *n*-butylamine (Figure S17b). This result indicates that π−π stacking[8,25] of aromatic amines with the P-Gc could play a vital role. Finally, we propose that, at first, carbonyl oxygen of β-diketo compounds interacts with the phosphoric acid group of P-Gc and then subsequent addition of amines takes place in the next step, which is followed by the elimination of water (Figure 5).[14]

Baeyer−Villiger Oxidation. The optimization of reaction conditions (Table 4) in the MW and OB was done using 4-*tert*-butylcyclohexanone (1 mmol), which produced white crystalline lactone (entries 1 to 3, Table 3) in various solvents. Acetonitrile was found to be suitable solvents over ethanol for both MW and OB techniques (Table 5). Non-coordinating solvents such as toluene and cyclohexane were found to be less effective in BV oxidation.

In contrast to aromatic ketones (like acetophenone), cyclic ketones were converted to their corresponding cyclic esters in good to high yields in a shorter reaction time (entry 3 vs entry 10 in acetonitrile, Table 4, Table 5). To get more conversion for aromatic ketones, we increased the reaction time up to 2 h, but then hydrolysis of the ester product was observed. Longer reaction times were needed for 2-adamantanone than for cyclohexanone (Table S8 and Figure S10d,e). The sterically congested transition state might be the possible reason. At room temperature (r.t.) in the OB, after 6 h, a 75% yield was observed for 4-*tert*-butylcyclohexanone. In the absence of P-Gc, no product was observed in both MW and OB conditions (entries 5 and 9, Table 4). Like β-ketoenamine synthesis,

https://dx.doi.org/10.1021/acsomega.0c01231
ACS Omega 2020, 5, 15962−15972

Table 3. Scheme and All Possible β-Ketoenamines with Yields ([a]MW and [b]OB)

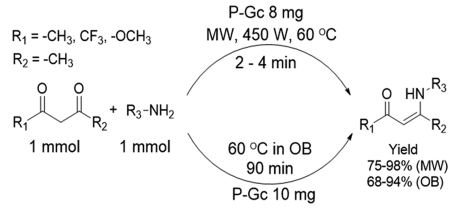

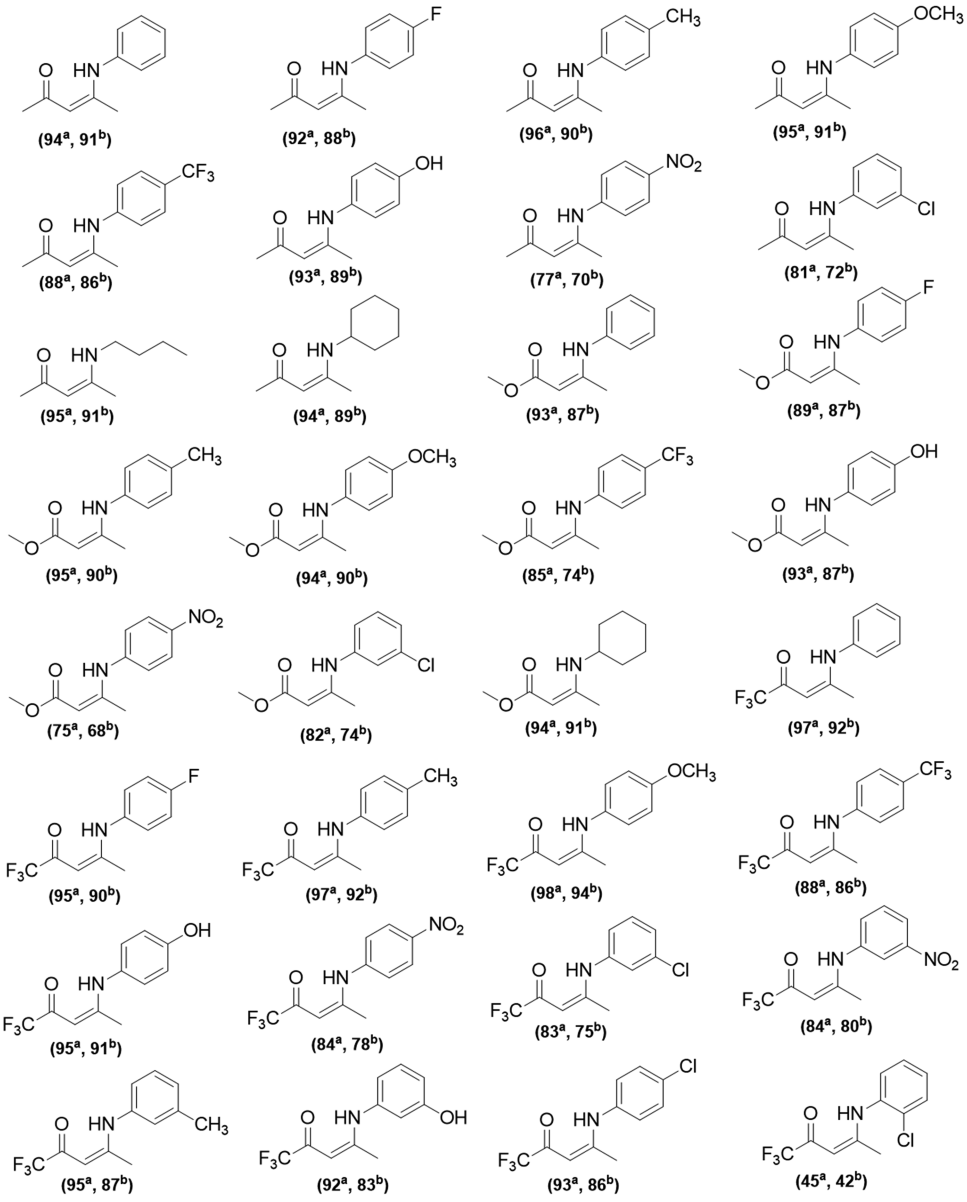

Baeyer–Villiger oxidation was also not a response with 1 mM H_3PO_4. P-Gc without an ultrasound effect also turned out to give a lesser yield for the conversion of cyclopentanone to δ-valerolactone and cyclohexanone to ε-caprolactone (Table S6).

Mechanistic Understanding of BV Oxidation Using P-Gc. The density functional theory calculations of the uncatalyzed BV reaction of acetone and H_2O_2 were performed previously.[28] These calculations revealed that, in the first step, H_2O_2 donates a hydrogen bond to the carbonyl oxygen and the formation of a Criegee intermediate proceeds via four-membered transition states (TS). Then, simultaneous proton transfer from the peroxyl oxygen and a nucleophilic attack of the peroxyl oxygen on the carbonyl carbon result in a five-membered TS. During this step, intramolecular rearrangement of a methyl group happens from the central carbon to the oxygen and, at the same time, the O–O bond is broken. The activation energy requirement for the uncatalyzed reaction was found to be very high (39.8 kcal/mol for Criegee intermediate formation and 41.7 kcal/mol for the BV rearrangement step).[29] For this reason, the BV oxidation of ketones with H_2O_2 does

https://dx.doi.org/10.1021/acsomega.0c01231
ACS Omega 2020, 5, 15962–15972

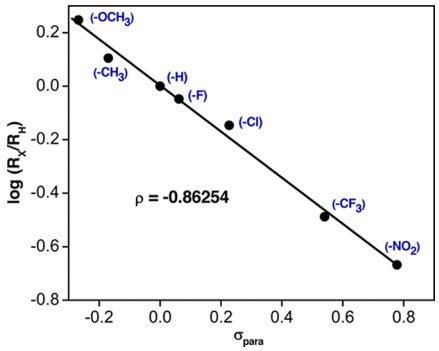

Figure 4. Hammett plot for reactions of different *para*-substituted anilines with 1,1,1-trifluoro-2,4-pentanedione.

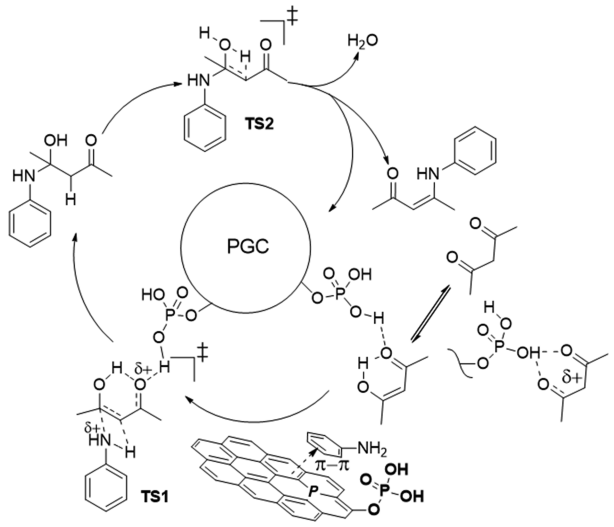

Figure 5. Proposed mechanism for P-Gc-catalyzed synthesis of *β*-ketoenamine.

Table 4. Optimization of Reaction Conditions for BV Oxidation

entry	P-Gc (mg)	temp (°C)	solvent	heating technique	yield (%)
1	8	80	acetonitrile	MW, 490 W, 6 min	20
2[a]	8	80	acetonitrile	MW, 700 W, 6 min	58
3[a]	15	80	acetonitrile	MW, 700 W, 6 min	84
4[a]	15	74	ethanol	MW, 700 W, 6 min	70
5[a]		80	acetonitrile	MW, 700 W, 6 min	00
6[a]	20	80	ethanol	OB, 2 h	55
7[a]	20	80	acetonitrile	OB, 2 h	81
8[a]	20	r.t.	acetonitrile	OB, 6 h	75
9[a]		80	acetonitrile	OB, 2 h	00
10[b]	15	95	acetonitrile	MW, 700 W, 50 min	58
11[b]	20	95	acetonitrile	OB, 9 h	55

[a]Cyclic ketones to lactones. [b]Aromatic ketones to esters.

not occur without catalytic activation. Carlqvist et al. reported that BF_3, a strong Lewis acid, helps reduce the activation barrier for both steps.[30] Sever et al. proposed that rearrangement of the chelated Criegee intermediate is the rate-determining step for the tin-catalyzed BV mechanism and the Lewis acidic Sn center facilitates departure of the hydroxyl leaving group.[31] Xu et al. reported that chiral phosphoric acid simultaneously increases the electrophilicity of the carbonyl

Table 5. Scheme and All Products of Baeyer–Villiger Oxidation with Yields[a,b,c]

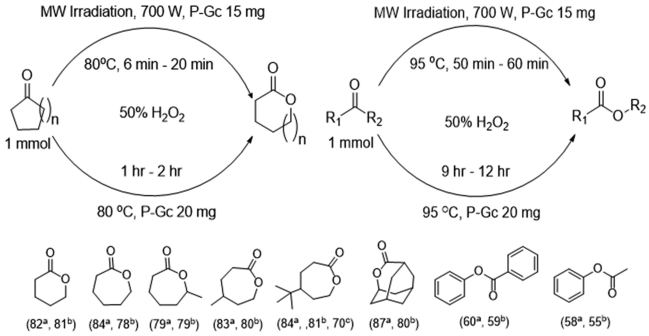

[a]Yield for MW-assisted synthesis in acetonitrile. [b]Yield for synthesis on OB in acetonitrile. [c]Yield for MW-assisted synthesis in ethanol.

carbon and nucleophilicity of hydrogen peroxide for enantioselective BV oxidation of 3-substituted cyclobutanones.[32] According to their report, the reaction did not go through a peroxyphosphoric acid intermediate. Here, our explanation is that the phosphoric acid functional groups present in P-Gc may increase the electrophilicity of the carbonyl group of the ketones to compensate for the weakness of the nucleophilicity of H_2O_2 and could lead toward a low-energy pathway through a Criegee adduction intermediate (Figure 6, path a).

However, in 2002, Berkessel et al. showed BV oxidation of ketones by H_2O_2 using catalytic Brønsted acids in hexafluoroisopropanol medium by a non-classical mechanism, via a spiro-bisperoxide intermediate.[33] To check whether this pathway exists or not in our case, we performed high-resolution mass spectrometry (HR-MS) during the course of the reaction. A spiro-bisperoxide compound (*m*/*z* calculated: 229.1435; observed: 229.1440) was trapped during oxidation of cyclohexanone (Figure 7). Similar intermediates were found in the reaction of 2-methylcyclohexanone and 4-methylcyclohexanone too. Therefore, the alternative mechanism could be the formation of lactonium cations from a spiro-bisperoxo intermediate followed by an attack of water at an acyl carbon atom (Figure 6, path b).[33,17b] Furthermore, adipic acid (~10%) (Figure S18d) and 6-hydroxyhexanoic acid (Figure S18c) were also isolated as byproducts. When we carried the reaction for more than 30 min in MW or 4 h in the OB, the predominant product was adipic acid, which supports its generation through either path c or d over oxidation of *ε*-caprolactone.[34] In MW conditions, we have also detected 2-cyclohexenone (Figure S18a) and octahydrobiphenylene-1,5(4b*H*,8b*H*)-dione (Figure S18b) in HR-MS as byproducts.[33] Octahydrobiphenylene-1,5(4b*H*,8b*H*)-dione is formed by a [2 + 2] cycloaddition reaction of 2-cyclohexenone.

Catalyst Recyclability. For up to five cycles of both *β*-ketoenamine synthesis and Baeyer–Villiger oxidation reactions, the recovered catalyst from the oil bath shows better recyclability than from microwave-assisted synthesis (Figure 8). After five cycles, the yield percentage of (*Z*)-1,1,1-trifluoro-4-((4-methoxy)phenylamino)pent-3-en-2-one dropped from 98 to 73 in MW. Similarly, the yield percentage of 5-(*tert*-butyl)oxepan-2-one dropped from 84 to 65 in MW after five cycles. For oil-bath reactions, no significant change for the yield percentage was observed across the five cycles for both of the reactions. After five cycles, recovered P-Gc was

https://dx.doi.org/10.1021/acsomega.0c01231
ACS Omega 2020, 5, 15962–15972

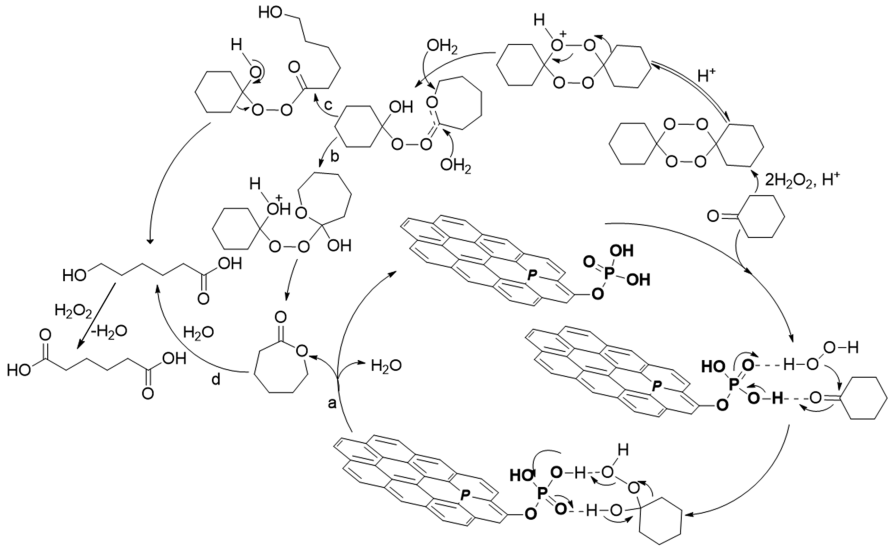

Figure 6. Proposed mechanism for the BV oxidation using P-Gc as a solid acid catalyst.

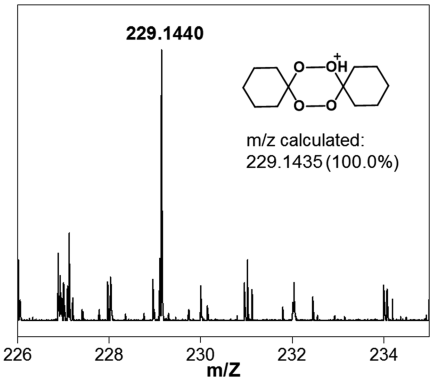

Figure 7. HR-MS data of spiro-bisperoxide trapped in the reaction mixture of cyclohexanone and hydrogen peroxide in MW conditions.

characterized through several techniques. No major change was observed in FTIR (Figure S11a), SEM (Figure S11b), TEM (Figure S11c,d), P-XRD (Figure S11e, peak shifted slightly to $2\theta = 24.704$, corresponding interlayer spacing = 3.60 Å, compared to 3.56 Å in the virgin P-Gc), and Raman (Figure S11f) analysis; however, the specific surface area was reduced from 1635 to 1048 m^2/g (BET analysis, Figure S12 and Table S9). A significant change was also observed in XPS analysis of recovered P-Gc after microwave treatment, indicating the drop of phosphorous contained to be from 3.18% (Table S5) to 1.55% (Table S10). These can be the reason for the gradual decrease of the activity of P-Gc. The increase of oxygen contained from 13.51 to 16.73% implies the partial oxidation of P-Gc during the reactions. Relative percentages of different functional groups (Table S11) from deconvoluted peaks (Figure S14) confirm the reduction of acid groups, including COOH and C−OH, which were present in trace amounts in virgin P-Gc. The increase of C−O functionalities and decrease of sp^2 C═C confirm the partial oxidation of C═C in the graphite plane.

Effect of Microwave Heating. Microwave heating is considered as a non-conventional energy source for organic synthesis. Compared to conventional heating, which is introduced in the sample from the surface, MW radiation is rapid and volumetric. The effect of microwave irradiation in chemical reactions is a combination of thermal and non-thermal effects.[35a] The magnitude of heating mostly depends on the dielectric losses of the molecules. In addition to this, Mingos has found that overheating in the range of 13−26 °C above the normal boiling point may occur in the case of polar liquids on using microwaves.[35b] This effect can be explained by

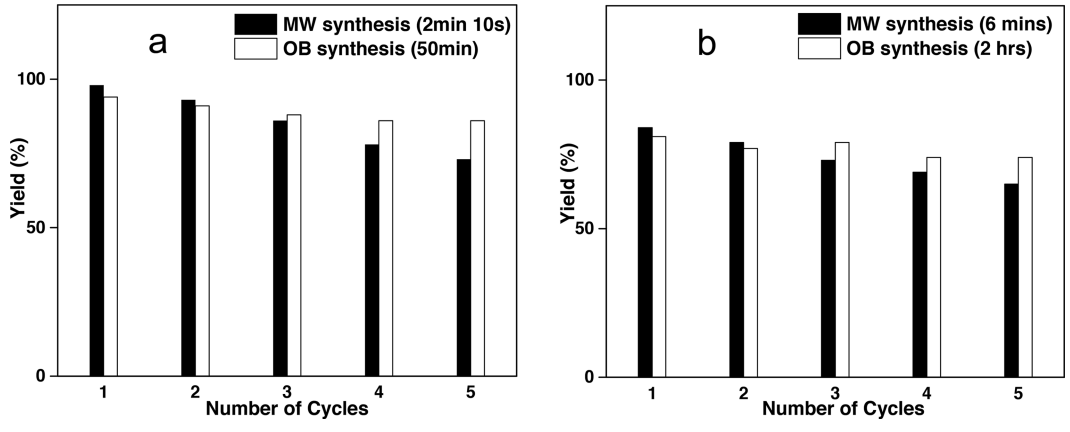

Figure 8. Recyclability of P-Gc in (a) β-ketoenamine synthesis and (b) BV oxidation.

https://dx.doi.org/10.1021/acsomega.0c01231
ACS Omega 2020, 5, 15962−15972

the "inverted heat transfer" effect since boiling nuclei are formed at the surface of the liquid. In our case also, a greater yield of was observed in polar solvent for both reactions.

CONCLUSIONS

In conclusion, we have successfully accomplished a green method for synthesis of β-ketoenamines in microwave using P-Gc as a solid acid catalyst (in comparison to previous reports; Table S13). In most cases, a ∼95% yield was achieved in ethyl acetate medium and the average reaction time was 3−5 min only. To the best of our knowledge, this is the fastest approach to date for β-ketoenamine synthesis using a heteroatom-doped carbocatalyst (Table S13). In solvent-free conditions, the yield of β-ketoenamines was ∼78%. Also, we are reporting for the first time BV oxidation by a heteroatom-doped graphitic material using H_2O_2 for a wide range of ketones in MW (in comparison to previous reports; Table S14).

ASSOCIATED CONTENT

Supporting Information

The Supporting Information is available free of charge at https://pubs.acs.org/doi/10.1021/acsomega.0c01231.

FTIR, BET, SEM, kinetics data, HPLC, HR-MS, NMR, etc. (PDF)

AUTHOR INFORMATION

Corresponding Author

Basab Bijayi Dhar − *Department of Chemistry, Shiv Nadar University, Dadri UP-201314, India;* orcid.org/0000-0002-8315-6291; Phone: + 91 9999872154; Email: basabbijayi@gmail.com, basab.dhar@snu.edu.in

Authors

Sayantan Maity − *Department of Chemistry, Shiv Nadar University, Dadri UP-201314, India;* orcid.org/0000-0002-5724-0190

Farsa Ram − *Polymer Science and Engineering Division, CSIR-National Chemical Laboratory, Pune, Maharashtra 411008, India*

Complete contact information is available at: https://pubs.acs.org/10.1021/acsomega.0c01231

Notes

The authors declare no competing financial interest.

ACKNOWLEDGMENTS

S.M. acknowledges Shiv Nadar University (SNU) for research fellowship, and F.R. acknowledges CSIR for research fellowship. B.B.D. acknowledges SNU for funding. The authors acknowledge Dr. Suneel Kumar for his help to use HR-TEM (FIST-supported) in IISER Bhopal, Dr. Sujit Deshmukh for AFM analysis, and Dr. Pratip Dutta for helpful discussion.

REFERENCES

(1) (a) Hu, C.; Dai, L. Doping of Carbon Materials for Metal-Free Electrocatalysis. *Adv. Mater.* **2019**, *31*, 1804672. (b) Zhao, S.; Wang, D.-W.; Amal, R.; Dai, L. Carbon-Based Metal-Free Catalysts for Key Reactions Involved in Energy Conversion and Storage. *Adv. Mater.* **2019**, *31*, 1801526. (c)) Paul, R.; Zhu, L.; Chen, H.; Qu, J.; Dai, L. Recent Advances in Carbon-Based Metal-Free Electrocatalysts. *Adv. Mater.* **2018**, *31*, 1806403. (d)) Ji, Y.; Dong, H.; Liu, C.; Li, Y. The progress of metal-free catalysts for the oxygen reduction reaction based on theoretical simulations. *J. Mater. Chem. A* **2018**, *6*, 13489. (e) Liu, X.; Dai, L. Carbon-Based Metal-Free Catalysts. *Nat. Rev. Mater.* **2016**, *1*, 1−12.

(2) (a) Hu, H.; Xin, J. H.; Hu, H.; Wang, X.; Kong, Y. Metal-free graphene-based catalyst-Insight into the catalytic activity: A short review. *Appl. Catal., A* **2015**, *492*, 1−9. (b) Daems, N.; Sheng, X.; Vankelecom, I. F. J.; Pescarmona, P. P. Metal-free doped carbon materials as electrocatalysts for the oxygen reduction reaction. *J. Mater. Chem. A* **2014**, *2*, 4085.

(3) (a) Varma, R. S. Greener and Sustainable Trends in Synthesis of Organics and Nanomaterials. *ACS Sustainable Chem. Eng.* **2016**, *4*, 5866−5878. (b) Baig, R. B. N.; Varma, R. S. Alternative energy input: mechanochemical, microwave and ultrasound-assisted organic synthesis. *Chem. Soc. Rev.* **2012**, *41*, 1559−1584. (c) Gawande, M. B.; Shelke, S. N.; Zboril, R.; Varma, R. S. Microwave-Assisted Chemistry: Synthetic Applications for Rapid Assembly of Nanomaterials and Organics. *Acc. Chem. Res.* **2014**, *47*, 1338−1348. (d) Namboodiri, V. V.; Varma, R. S. Solvent-Free Sonochemical Preparation of Ionic Liquids. *Org. Lett.* **2002**, *4*, 3161−3163.

(4) Varma, R. S. Clay and clay-supported reagents in organic synthesis. *Tetrahedron* **2002**, *58*, 1235−1255.

(5) (a) Shang, S. S.; Gao, S. Heteroatom−Enhanced Metal−Free Catalytic Performance of Carbocatalysts for Organic Transformations. *ChemCatChem* **2019**, *11*, 3730−3744. (b) Higgins, D.; Zamani, P.; Yu, A.; Chen, Z. The application of graphene and its composites in oxygen reduction electrocatalysis: a perspective and review of recent progress. *Energy Environ. Sci.* **2016**, *9*, 357−390. (c) Navalon, S.; Dhakshinamoorthy, A.; Alvaro, M.; Garcia, H. Carbocatalysis by Graphene-Based Materials. *Chem. Rev.* **2014**, *114*, 6179−6212.

(6) (a) Garrido-Barros, P.; Gimbert-Suriñach, C.; Moonshiram, D.; Picón, A.; Monge, P.; Batista, V. S.; Llobet, A. Electronic π-Delocalization Boosts Catalytic Water Oxidation by Cu(II) Molecular Catalysts Heterogenized on Graphene Sheets. *J. Am. Chem. Soc.* **2017**, *139*, 12907−12910. (b) Su, C.; Loh, K. P. Carbocatalysts: Graphene Oxide and Its derivatives. *Acc. Chem. Res.* **2012**, *46*, 2275−2285.

(7) Gao, Y.; Hu, G.; Zhong, J.; Shi, Z.; Zhu, Y.; Su, D. S.; Wang, J.; Bao, X.; Ma, D. Nitrogen-Doped sp^2-Hybridized Carbon as a Superior Catalyst for Selective Oxidation. *Angew. Chem. Int. Ed.* **2013**, *52*, 2109−2113.

(8) Vijaya Sundar, J.; Subramanian, V. Novel Chemistry for the Selective Oxidation of Benzyl Alcohol by Graphene Oxide and N-Doped Graphene. *Org. Lett.* **2013**, *15*, 5920−5923.

(9) (a) Matthews, P. D.; King, T. C.; Glass, H.; Magusin, P. C. M. M.; Tustin, G. J.; Brown, P. A. C.; Cormack, J. A.; García-Rodríguez, R.; Leskes, M.; Dutton, S. E.; Barker, P. D.; Grosche, F. M.; Alavi, A.; Grey, C. P.; Wright, D. S. Synthesis and extensive characterisation of phosphorus doped graphite. *RSC Adv.* **2016**, *6*, 62140−62145. (b) Ghafuri, H.; Talebi, M. Water-Soluble Phosphated Graphene: Preparation, Characterization, Catalytic Reactivity, and Adsorption Property. *Ind. Eng. Chem. Res.* **2016**, *55*, 2970−2982. (c) Duan, J.; Chen, S.; Jaroniec, M.; Qiao, S. Z. Heteroatom-Doped Graphene-Based Materials for Energy-Relevant Electrocatalytic Processes. *ACS Catal.* **2015**, *5*, 5207−5234. (d) Wang, X.; Sun, G.; Routh, P.; Kim, D.-H.; Huang, W.; Chen, P. Heteroatom-doped graphene materials: syntheses, properties and applications. *Chem. Soc. Rev.* **2014**, *43*, 7067−7098.

(10) Patel, M. A.; Luo, F.; Khoshi, M. R.; Rabie, E.; Zhang, Q.; Flach, C. R.; Mendelsohn, R.; Garfunkel, E.; Szostak, M.; He, H. P-Doped Porous Carbon as Metal Free Catalysts for Selective Aerobic Oxidation with an Unexpected Mechanism. *ACS Nano* **2016**, *10*, 2305−2315.

(11) Eshghi, H.; Seyedi, S. M.; Safaei, E.; Vakili, M.; Farhadipour, A.; Bayat-Mokhtari, M. Silica supported $Fe(HSO_4)_3$ as an efficient, heterogeneous and recyclable catalyst for synthesis of β-enaminones and β-enamino esters. *J. Mol. Catal. A: Chem.* **2012**, *363-364*, 430−436.

(12) Salama, N. N.; Scott, K. R.; Eddington, N. D. DM27, an Enaminone, Modifies the *In Vitro* Transport of Antiviral Therapeutic Agents. *Biopharm. Drug Dispos.* **2004**, *25*, 227−236.

(13) (a) Xu, S.-L.; Li, C.-P.; Li, J.-H. Solid-State Synthesis of β-Enamino Ketones from Solid 1,3-Dicarbonyl Compounds and Ammonium Salts or Amines. *Synlett* **2009**, *2009*, 818−822. (b) Dannhardt, G.; Bauer, A.; Nowe, U. Non−steroidal anti−inflammatory agents. Part 23. Synthesis and Pharmacological Activity of Enaminones which Inhibit both Bovine Cyclooxygenase and 5-Lipoxygenase. *J. Prakt. Chem.* **1998**, *340*, 256−263.
(14) Deng, D.; Xiao, L.; Chung, I.-M.; Kim, I. S.; Gopiraman, M. Industrial-Quality Graphene Oxide Switched Highly Efficient Metal and Solvent-Free Synthesis of β-Ketoenamines under Feasible Conditions. *ACS Sustainable Chem. Eng.* **2017**, *5*, 1253−1259.
(15) Kumar, A.; Rout, L.; Dhaka, R. S.; Samal, S. L.; Dash, P. Design of a graphene oxide-SnO_2 nanocomposite with superior catalytic efficiency for the synthesis of β-enaminones and β-enaminoesters. *RSC Adv.* **2015**, *5*, 39193−39204.
(16) (a) Zhang, X.; Yang, H.; Yang, G.; Li, S.; Wang, X.; Ma, J. Metal-Free Mesoporous SiO_2 Nanorods as a Highly Efficient Catalyst for the Baeyer-Villiger Oxidation under Mild Conditions. *ACS Sustainable Chem. Eng.* **2018**, *6*, 5868−5876. (b) Kotlewska, A. J.; van Rantwijk, F.; Sheldon, R. A.; Arends, I. W. C. E. Epoxidation and Baeyer−Villiger oxidation using hydrogen peroxide and a lipase dissolved in ionic liquids. *Green Chem.* **2011**, *13*, 2154−2160.
(17) (a) Uyanik, M.; Ishihara, K. Baeyer−Villiger Oxidation Using Hydrogen Peroxide. *ACS Catal.* **2013**, *3*, 513−520. (b) ten Brink, G.-J.; Arends, I. W. C. E.; Sheldon, R. A. The Baeyer−Villiger Reaction: New Developments toward Greener Procedures. *Chem. Rev* **2004**, *104*, 4105−4124.
(18) (a) Huang, S.; Cheong, L.-Z.; Wang, D.; Shen, C. Nanostructured Phosphorus Doped Silicon/Graphite Composite as Anode for High-Performance Lithium-Ion Batteries. *ACS Appl. Mater. Interfaces* **2017**, *9*, 23672−23678. (b) Quan, B.; Yu, S.-H.; Chung, D. Y.; Jin, A.; Park, J. H.; Sung, Y.-E.; Piao, Y. Single Source Precursor-based Solvothermal Synthesis of Heteroatom-doped Graphene and Its Energy Storage and Conversion Applications. *Sci. Rep.* **2015**, *4*, 5639. (c) Marcano, D. C.; Kosynkin, D. V.; Berlin, J. M.; Sinitskii, A.; Sun, Z.; Slesarev, A.; Alemany, L. B.; Lu, W.; Tour, J. M. Improved Synthesis of Graphene Oxide. *ACS Nano* **2010**, *4*, 4806−4814.
(19) (a) Daasch, L.; Smith, D. Infrared Spectra of Phosphorus Compounds. *Anal. Chem.* **1951**, *23*, 853−868. (b) Li, Y.; Li, S.; Wang, Y.; Wang, J.; Liu, H.; Liu, X.; Wang, L.; Liu, X.; Xue, W.; Ma, N. Electrochemical Synthesis of Phosphorus-doped graphene Quantum Dots for free radical scavenging. *Phys. Chem. Chem. Phys.* **2017**, *19*, 11631−11638.
(20) (a) Saito, R.; Hofmann, M.; Dresselhaus, G.; Jorio, A.; Dresselhaus, M. S. Raman spectroscopy of graphene and carbon nanotubes. *Adv. Phys.* **2011**, *60*, 413−550. (b) Dresselhaus, M. S.; Jorio, A.; Souza Filho, A. G.; Saito, R. Defect characterization in graphene and carbon nanotubes using Raman spectroscopy. *Phil. Trans. R. Soc. A* **2010**, *368*, 5355−5377. (c) Ferrari, A. C.; Robertson, J. Interpretation of Raman spectra of disordered and amorphous carbon. *Phys. Rev. B* **2000**, *61*, 14095−14107.
(21) (a) An, M.; Du, C.; Du, L.; Sun, Y.; Wang, Y.; Chen, C.; Han, G.; Yin, G.; Gao, Y. Phosphorus-doped graphene support to enhance electrocatalysis of methanol oxidation reaction on platinum nanoparticles. *Chem. Phys. Lett.* **2017**, *687*, 1−8. (b) Zhang, C.; Mahmood, N.; Yin, H.; Liu, F.; Hou, Y. Synthesis of Phosphorus-Doped Graphene and its Multifunctional Applications for Oxygen Reduction Reaction and Lithium Ion Batteries. *Adv. Mater.* **2013**, *25*, 4932−4937. (c) Hou, H.; Shao, L.; Zhang, Y.; Zou, G.; Chen, J.; Ji, X. Large-Area Carbon Nanosheets Doped with Phosphorus: A High-Performance Anode Material for Sodium-Ion Batteries. *Adv. Sci.* **2017**, *4*, 1600243.
(22) (a) Guo, F.; Creighton, M.; Chen, Y.; Hurt, R.; Külaots, I. Porous structures in stacked, crumpled and pillared graphene-based 3D materials. *Carbon* **2014**, *66*, 476−484. (b) Lu, W.; Hartman, R.; Qu, L.; Dai, L. Nanocomposite Electrodes for High-Performance Supercapacitors. *J. Phys. Chem. Lett.* **2011**, *2*, 655−660. (c) Baughman, R. H.; Zakhidov, A. A.; de Heer, W. A. Carbon Nanotubes − the Route Toward Applications. *Science* **2002**, *297*, 787−792.
(23) Textor, M.; Ruiz, L.; Hofer, R.; Rossi, A.; Feldman, K.; Hähner, G.; Spencer, N. D. Structural Chemistry of Self-Assembled Monolayers of Octadecylphosphoric Acid on Tantalum Oxide Surfaces. *Langmuir* **2000**, *16*, 3257−3271.
(24) Hellweg, S.; Fischer, U.; Scheringer, M.; Hungerbühler, K. Environmental assessment of chemicals: methods and application to a case study of organic solvents. *Green Chem.* **2004**, *6*, 418−427.
(25) (a) Ganesh Babu, S.; Thomas, B.; Nijamudheen, A.; Datta, A.; Karvembu, R. Cu/AlO(OH)-catalyzed formation of β-enamino ketones/esters under solvent, ligand and base free conditions − experimental and computational studies. *Catal. Sci. Technol.* **2012**, *2*, 1872−1878. (b) Kidwai, M.; Bhardwaj, S.; Mishra, N. K.; Bansal, V.; Kumar, A.; Mozumdar, S. A novel method for the synthesis of β-enaminones using Cu-nanoparticles as catalyst. *Catal. Commun* **2009**, *10*, 1514−1517.
(26) (a) Lienhard, G. E.; Wang, T. C. Mechanism of Acid-catalyzed enolization of ketones. *J. Am. Chem. Soc.* **1969**, *91*, 1146−1153. (b) Cederstav, A. K.; Novak, B. M. Investigations into the Chemistry of Thermodynamically Unstable Species. The direct polymerization of Vinyl Alcohol, the Enolic Tautomer of Acetaldehyde. *J. Am. Chem. Soc.* **1994**, *116*, 4073−4074. (c) Iglesias, E. Determination of keto−enol equilibrium constants and the kinetic study of the nitrosation reaction of β-dicarbonyl compounds. *J. Chem. Soc., Perkin Trans. 2* **1997**, *3*, 431−440. (d) Bertolasi, V.; Ferretti, V.; Gilli, P.; Yao, X.; Li, C.-J. Substituent effects on keto−enol tautomerization of β-diketones from X-ray structural data and DFT calculations. *New J. Chem.* **2008**, *32*, 694−704.
(27) (a) Björk, J.; Hanke, F.; Palma, C.-A.; Samori, P.; Cecchini, M.; Persson, M. Adsorption of Aromatic and Anti-Aromatic Systems on Graphene through π-π Stacking. *J. Phys. Chem. Lett.* **2010**, *1*, 3407−3412. (b) Zhang, Z.; Huang, H.; Yang, X.; Zang, L. Tailoring Electronic Properties of Graphene by π-π Stacking with Aromatic Molecules. *J. Phys. Chem. Lett.* **2011**, *2*, 2897−2905.
(28) (a) Uyanik, M.; Nakashima, D.; Ishihara, K. Baeyer−Villiger Oxidation and Oxidative Cascade Reactions with Aqueous Hydrogen Peroxide Catalyzed by Lipophilic $Li[B(C_6F_5)_4]$ and $Ca[B(C_6F_5)_4]_2$. *Angew. Chem. Int. Edit.* **2012**, *51*, 9093−9096. (b) Peris, G.; Miller, S. J. A Nonenzymatic Acid/Peracid Catalytic Cycle for the Baeyer-Villiger Oxidation. *Org. Lett.* **2008**, *10*, 3049−3052. (c) Hao, X.; Yamazaki, O.; Yoshida, A.; Nishikido, J. Green Baeyer−Villiger oxidation with hydrogen peroxide: $Sn[N(SO_2C_8F_{17})_2]_4$ as a highly selective Lewis acid catalyst in a fluorous biphase system. *Green Chem.* **2003**, *5*, 524−528.
(29) Bach, R. D. The Role of Acid Catalysis in the Baeyer−Villiger Reaction. A Theoretical Study. *J. Org. Chem.* **2012**, *77*, 6801−6815.
(30) Carlqvist, P.; Eklund, R.; Brinck, T. A Theoretical Study of the Uncatalyzed and BF3-Assisted Baeyer-Villiger Reactions. *J. Org. Chem.* **2001**, *66*, 1193−1199.
(31) Sever, R. R.; Root, T. W. Computational Study of Tin-Catalyzed Baeyer-Villiger Reaction Pathways Using Hydrogen Peroxide as Oxidant. *J. Phys. Chem. B.* **2003**, *107*, 10848−10862.
(32) Xu, S.; Wang, Z.; Zhang, X.; Zhang, X.; Ding, K. Chiral Brønsted Acid Catalyzed Asymmetric Baeyer−Villiger Reaction of 3-Substituted Cyclobutanones by Using Aqueous H_2O_2. *Angew. Chem. Int. Ed.* **2008**, *47*, 2840−2843.
(33) Berkessel, A.; Andreae, M. R. M.; Schmickler, H.; Lex, J. Baeyer-Villiger Oxidations with Hydrogen Peroxide in Fluorinated Alcohols: Lactone Formation by a Nonclassical Mechanism. *Angew. Chem. Int. Edit.* **2002**, *41*, 4481−4484.
(34) Cavani, F.; Raabova, K.; Bigi, F.; Quarantelli, C. A Rationale of the Baeyer−Villiger Oxidation of Cyclohexanone to ε-Caprolactone with Hydrogen Peroxide: Unprecedented Evidence for a Radical Mechanism Controlling Reactivity. *Chem. − Eur. J.* **2010**, *16*, 12962−12969.
(35) (a) de la Hoz, A.; Díaz-Ortiz, Á.; Moreno, A. Microwaves in organic synthesis. Thermal and non-thermal microwave effects. *Chem. Soc. Rev.* **2005**, *34*, 164−178. (b) Baghurst, D. R.; Mingos, D. M. P.

https://dx.doi.org/10.1021/acsomega.0c01231
ACS Omega 2020, 5, 15962−15972

Superheating effects associated with microwave dielectric heating. *J. Chem. Soc., Chem. Commun.* **1992**, 674−677.

https://dx.doi.org/10.1021/acsomega.0c01231
ACS Omega 2020, 5, 15962−15972